Seismic Vulnerability Assessment of Ageing Reinforced Concrete Structures under Real Mainshock-Aftershock Ground Motions

Ebrahim Afsar Dizaj[a*], Mohammad R. Salami[b], Mohammad M Kashani[c]

[a]Assistant Professor, Department of Civil Engineering, Azarbaijan Shahid Madani University, Tabriz, Iran. (corresponding author), Email: ebrahim.afsardizaj@azaruniv.ac.ir

Address: Iran, Tabriz, Azarbaijan Shahid Madani University, Faculty of Engineering, Department of Civil Engineering
Phone number: +989141581825

ORCID: https://orcid.org/0000-0002-7755-9983

[b]Lecturer in Engineering, School of Engineering and the Built Environment, Birmingham City University, B5 5JU, United Kingdom, Email: mohammad.salami@bcu.ac.uk

ORCID: https://orcid.org/0000-0003-0429-5398

[c]Associate Professor, Faculty of Engineering and Physical Sciences, University of Southampton, Southampton, SO17 1BJ, United Kingdom, Email: mehdi.kashani@soton.ac.uk

ORCID: https://orcid.org/0000-0003-0008-0007

Seismic Vulnerability Assessment of Ageing Reinforced Concrete Structures under Real Mainshock-Aftershock Ground Motions

Ebrahim Afsar Dizaj[a*], Mohammad R. Salami[b], Mohammad M. Kashani[c]

[a]Assistant Professor, Department of Civil Engineering, Azarbaijan Shahid Madani University, Tabriz, Iran. (corresponding author), Email: ebrahim.afsardizaj@azaruniv.ac.ir

[b]Lecturer in Engineering, School of Engineering and the Built Environment, Birmingham City University, B5 5JU, United Kingdom, Email: mohammad.salami@bcu.ac.uk

[c]Associate Professor, Faculty of Engineering and Physical Sciences, University of Southampton, Southampton, SO17 1BJ, United Kingdom, Email: mehdi.kashani@soton.ac.uk

Abstract

Ageing structures located in moderate to high seismicity regions are exposed to multiple natural stressors during their lifetime. Large earthquake events coupled with environmental aggressive agents increase the progressive failure probability of these structures. The accumulated damage during the main earthquake event might be exacerbated by its following aftershocks. This might result in catastrophic failure of these structures, and consequently, result in several socio-economic losses. Taking such progressive deterioration mechanism into consideration, the current study presents a framework to assess the vulnerability of ageing Reinforced Concrete (RC) frames subject to real Mainshock-Aftershock (MS-AS) ground motion sequences. Employing an advanced fibre-based finite element modelling technique, the nonlinear static and dynamic behaviour of a case-study RC frame with various ages is simulated under 48 real MS-AS record pairs. Quantifying corrosion-variant damage states, the age-specific fragility curves are developed for the considered structure under both single MS events and MS-AS sequences. It was found that the severely corroded RC frames are most likely to collapse before the second event comes up. Moreover, results show that the PGA ratio of AS to MS plays a critical role in seismic vulnerability assessment of highly corrosion-damaged RC frames.

Keywords: mainshock-aftershock; reinforced concrete; corrosion; IDA; fragility; vulnerability assessment

1. Introduction

In recent years, the catastrophic collapse of ageing RC structures/infrastructures has been one of the main challenging engineering problems (Lee et al., 2013; Reggia et al., 2020). There are numerous ageing concrete structures worldwide suffering from chloride-induced corrosion of reinforcements (Virmani, 2002; Wallbank, 1989). The capacity reduction of these structures might endanger people's life, rise rehabilitation and maintenance costs, and result in several socio-economic consequences (Panchireddi & Ghosh, 2019). The problem is much more complicated for the ageing structures that are prone to natural disasters, like large earthquakes. The previously conducted survey shows that a large number of corrosion-damaged RC structures are located in moderate to high seismicity regions; where the structures have experienced/might experience multiple earthquakes during their service lifetime (FHWA, 2015).

Generally, in each earthquake event, a chain of Foreshocks (FS), Mainshock (MS) and Aftershocks (AS) takes place. Several disastrous collapses due to strong earthquakes that were followed by smaller magnitude events (AS) occurred in the past few decades. For example, while a RC building in Turkey was slightly damaged under the first event of 1999 Kocaeli earthquake (with Mw=7.4); it was completely collapsed under the subsequent damaging aftershock (with Mw=5.9) (Jeon et al., 2015). More recent damaging Mainshock-Aftershock (MS-AS) events also occurred throughout the globe, such as 2010 Haiti earthquake, 2010 Darfield earthquake (in Newzeland), 2011 Tohoku earthquake (in Japan), 2012 Emilia earthquake (in Italy), 2012 Varzgan and 2017 Kermanshah earthquakes (in Iran) (Jeon et al., 2015; Manafpour & Moghaddam, 2019; Raghunandan et al., 2015; Salami et al., 2019).

While in a great number of studies the seismic vulnerability of structures is assessed considering the single MS(s) event, such assessments considering MS-AS sequences have received significant attention over the previous decade (Acito et al., 2014, 2020; Chase et al., 2019; Goda & Taylor, 2012; Hatzivassiliou & Hatzigeorgiou, 2015; Hatzigeorgiou & Liolios, 2010; Hosseinpour & Abdelnaby, 2017;

Iervolino et al., 2020; Jalayer et al., 2011; Jeon et al., 2015; Naderpour & Vakili, 2019; Raghunandan et al., 2015). Using real and synthetic MS-AS sequences (generated based on Omori's law (Shcherbakov et al., 2005)), Goda and Taylor (2012) investigated the extent of additional damage caused by AS. They found that, while the real MS-AS sequences increase the damage of structure by less than 10% (comparing to MS only); this increase is estimated as 30-40 % using synthetic MS-AS records. Jeon et al. (2015) investigated the post-MS damage of older California RC frames. It was found that frames that exhibit larger damages during the initial event are much more vulnerable under the subsequent event (Jeon et al., 2015). Employing numerical MDOF models, Raghunandan et al. (2015) studied the AS vulnerability of modern RC frames located in California. The findings of Raghunandan et al. (2015) show that the AS vulnerability of structures is highly dependent on the extent of structural damage during the MS event. For example, if the structure shows slight damage during MS, its vulnerability wouldn't be significantly affected during associated AS.

Recently, life-cycle seismic resilience and vulnerability of transportation bridge network have been studied under multiple hazards (Capacci & Biondini, 2020; Capacci et al., 2020). The findings of Capacci et al. (2020) suggest that aggressive environment adversely affect the seismic performance and functionality resilience of highway bridges. Moreover, the seismic exposure condition can significantly affect the decay in time of resilience of ageing infrastructures. Titi et al. (2018) investigated the life-cycle seismic performance of a three-storey corroded RC frame considering different exposure scenarios in a probabilistic platform. They found that the exposure scenario plays a critical role for low to moderate exposure, but for severe exposures the damage process is not significantly affected by the level of surface chloride concentration. The state-of-the-art studies associated with the multi-hazard resilience of highway bridge networks has been reviewed by Banerjee et al. (2019).

In the literature, a significant deal of research has been dedicated to evaluating the seismic performance of corrosion-damaged RC structures (Dizaj et al., 2018a, 2018b; Dizaj & Kashani, 2020; F. Cui et al.,

2018; Z. Cui et al., 2019; Ge et al., 2020; Guo et al., 2015; Xu et al., 2020). The outcome of these studies confirms that depending on the level of corrosion, the structural capacity (both the strength and ductility) and energy dissipation capacity of these structures are significantly decreased; and therefore, they are deteriorated significantly under repeated cyclic loading. More specifically, Dizaj et al. (2018a) demonstrated that Damage Limit States (DLS) of corroded RC structures should be considered as corrosion-variant parameters as they significantly decrease over their service life. However, all of these studies have been conducted based on the single ground motion event, (i.e. MS event). Considering that, during the same event the corroded RC structures will exhibit larger damage comparing to intact structure; the post-MS events might significantly intensify the previously accumulated damage. Therefore, disregarding the additional damage due to the subsequent AS events might considerably underestimate the seismic vulnerability of deteriorated RC structures.

In a recent study, Panchireddi and Ghosh (2019) investigated the cumulative vulnerability of highway bridges subjected to multiple mainshocks. Panchireddi and Ghosh (2019) found that corrosion highly increases the vulnerability of RC bridges under multiple earthquakes. In another study in the same area, Cui et al. (2019) found that multiple earthquake events expedite the corrosion process, and therefore, influence the vulnerability of RC bridge piers. However, these studies had several limitations. For instance, the effect of corrosion damage on DLS, inelastic buckling behaviour and low-cycle fatigue degradation of steel reinforcements were disregarded. Additionally, the main focus of these studies was multiple earthquakes (artificial MS-AS pairs); that is inherently different from as recorded real MS-AS sequences.

1.2 Research contribution and novelty

The above discussion shows that there is a significant scarcity in the literature to evaluate the seismic vulnerability of RC structures considering the environmental aggressive agents coupled with real natural sequential disasters (i.e. MS-AS sequences). Therefore, the main contribution of the this studyis to

investigate the seismic vulnerability of ageing RC frames that are prone to successive real MS-AS events. Fuertehrmore, in all the previous studies (Panchireddi and Ghosh (2019)) a simple fibre beam-column model that did not account for inelastic buckling and low-cycle fatigue of resisnformencet has been used. Therefore, the impact of material cyclic degrdataion together with corrosion and MS_AS sequences could not be investigated. Moreover, the ground motions used in this study are real ground motions, which are select using conditional mean spectrum. These ground motions are taken from a unique grund motion database, which is the only existing ground motions that combine real data from PEER-NGA and Japanese K-NET/KiK-net for seismic performance assessment of structures under MS-AS sequences

Figure 1 shows a general view of the proposed framework for seismic vulnerability assessment of deteriorated RC structures subject to real MS-AS events. As Figure 1 shows, the whole paper is comprised of three main phases, such as: 1) Nonlinear Finite Element (NFE) modelling and quantification of corrosion-variant DLS; 2) MS-AS ground motion record selection based on Conditional Mean Spectrum (CMS) method, and 3) MS-AS IDAs, damage evaluation and fragility assessment. The first two phases (phases 1&2) are based on the existing studies and models (including the previous studies of the authors (Dizaj et al., 2018a, 2018b)), and phase 3 presents the main contribution of the current study.

Phase 1 in Figure 1 is covered in sections 2 to 4. The structural details of case-study RC frame are presented in section 2; section 3 describes the numerical model and advanced NFE modelling methodology, and section 4 discusses the evaluation of corrosion-variant DLS using monotonic pushover analysis on pristine and deteriorated RC frames. Phase 2 of Figure 1 is covered in section 5. Using CMS as a target spectrum, a suite of real MS-AS record pairs for the site of the case-study structure is selected, which is discussed in section 5. Finally, Phase 3 of Figure 1 is covered in section 6. Section 6.1 discusses the IDAs of MSAS ground motions on both the pristine and deteriorated frames. Using the IDA outputs, different sources of damages are evaluated and the structure-specific corrosion-variant MS-AS fragility curves are developed, which are discussed in section 6.2 and 6.3 respectively. Moreover, in section 6.4,

the effect of PGA ratio of AS to MS on nonlinear dynamic behaviour and fragility of case-study RC frames is investigated. It is found that the PGA ratio of AS to MS is a key factor in the fragility assessment of ageing structures. The paper ends with discussions on the results, highlighting remarks and areas for future studies.

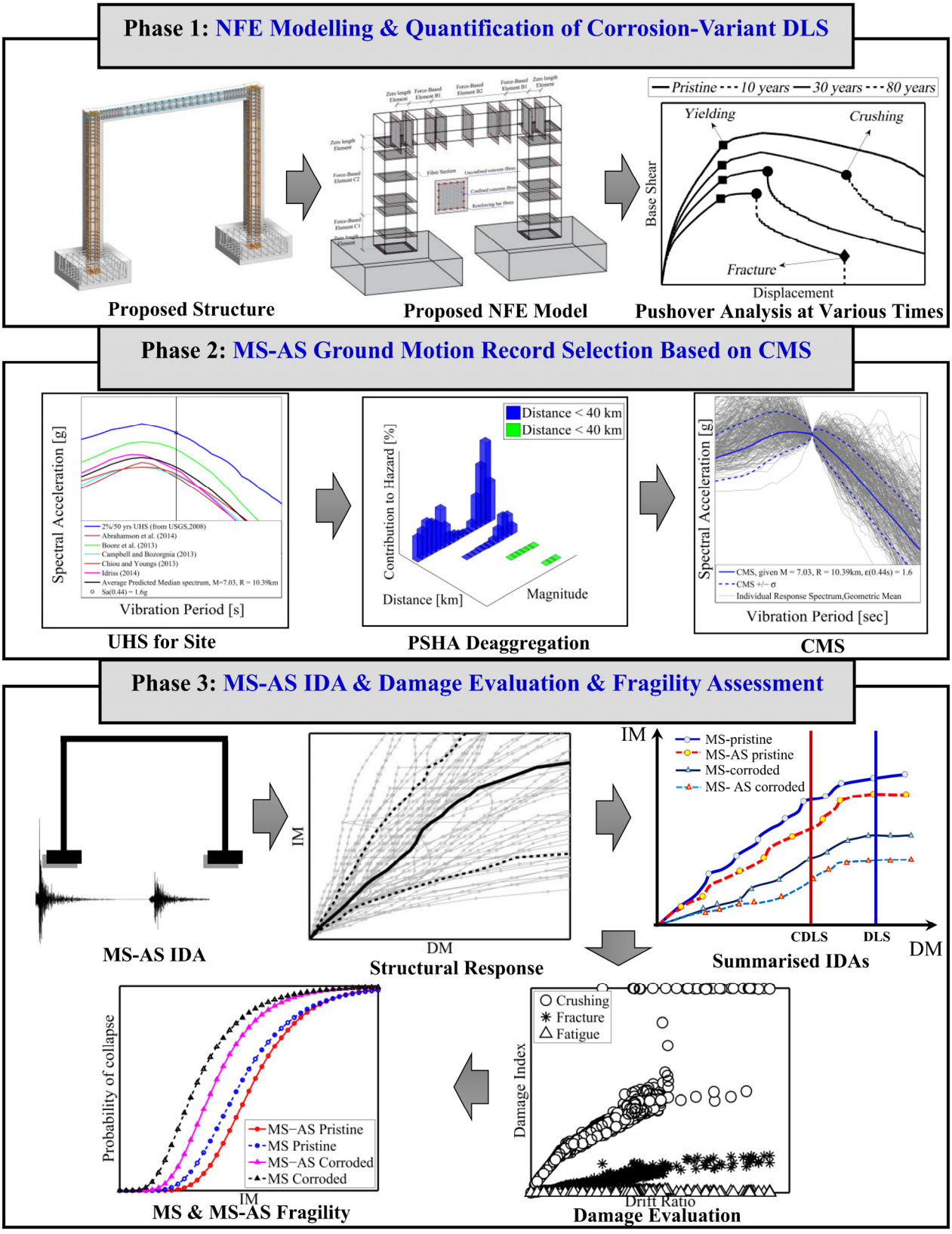

Figure 1. Proposed framework for seismic vulnerability assessment of ageing RC frames under real MS-AS sequences

2. Case-study RC frame

De-passivation of the protective thin oxide film of the reinforcing steel, in coastal areas and marine environment where high chloride levels are found, results in corrosion initiation (Val, 2007; Vu and Stewart, 2000). The corrosion level of reinforcement is typically described in term of mass loss percentage, ψ. ψ is a function of time from corrosion initiation t_p, water to cement ratio w/c, concrete cover from the surface of reinforcing bars d_c and diameter of reinforcement d, as represented in Equation (1) (Stewart and Suo, 2009; Vu and Stewart, 2000):

$$\psi(t_p, w/c, d_c, d) = \left[1 - \left(\frac{d - 1.05 \times (1 - w/c)^{-1.64} \times t_p^{0.71}}{d_c \times d}\right)^2\right] \times 100 \quad (1)$$

It should be noted that the focus of this study is on the duration after corrosion initiation, and hence, chloride ions have a negligible impact on the corrosion rate (Otieno et al. 2016a, 2016b; Vu and Stewart, 2000).

In this study, a seismically designed one story-one bay RC moment frame is considered as a case study structure to conduct nonlinear analyses. The frame is considered to be located in high seismicity and aggressive environment in California, US. The proposed frame is designed to meet the requirements of ASCE 7–02 (2002) and ACI 318–02 (2002). The design axial force (including the dead load of the roof plus 20% of design live load) on top of each column is assumed to be 280 KN. The spacing of ties at the top and bottom critical regions of the columns are considered to be 100 mm, and for out of these regions it is considered to be 200 mm. The spacing of ties at the left and right critical regions of the beam is considered to be 80 mm, and for the non-critical region, it is considered to be 150 mm. Figure 2 shows a schematic 3D view of the considered RC frame. The structural and geometrical details of the hypothetical frame are provided in Table 1, and the material parameters are presented in Table 2. It should be noted that the cross-sectional shape of both the columns and beam is square.

The hypothetical frame is assumed to be in four different ages: *i*) Frame A, the pristine frame (t_p=0); *ii*) Frame B, slightly corroded frame (t_p=10 years); *iii*) Frame C, moderately corroded frame (t_p=40 years); and *iv*) Frame D, severely corroded frame (t_p=100). It should be noted that the corrosion condition of each frame is expressed based on the values of calculated mass loss percentages (at each age) tabulated in Table 3. Furthermore, *w/c* is assumed as 0.5, and d_c as 30 mm and 40 mm for stirrups and longitudinal bars, respectively. The estimated mass loss percentages will be used in the next sections of the paper to modify the mechanical characteristics of steel and concrete materials.

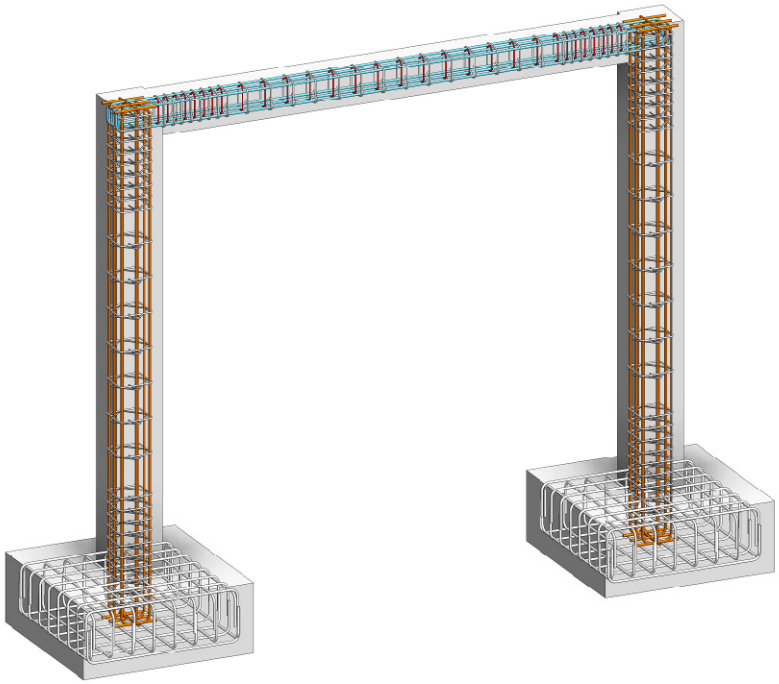

Figure 2. 3D view of the case-study RC frame

Table 1. Structural details of the hypothetical RC frame

Parameter	Symbol	Value	Unit
Column width	B_c	400	mm
Beam width	B_h	300	mm
Column height	H	4000	mm
Beam length	L	5000	mm
Longitudinal reinforcement ratio of column	ρ_l	0.0157	-
Top longitudinal reinforcement ratio of beam	ρ_{top}	0.0073	-
Bottom longitudinal reinforcement ratio of beam	ρ_{bot}	0.0073	-
Volumetric ratio of transverse reinforcement of column	ρ_v	0.0209	-
Ratio of transverse reinforcement of beam	ρ_s	0.0147	-

Table 2. Mechanical properties of reinforcing bars and concrete

Parameter	Symbol	Value	Unit
Yield strength of longitudinal reinforcement	f_{yl}	420	MPa
Yield strength of transverse reinforcement	f_{yh}	300	MPa
Elastic modulus	E_s	210000	MPa
Fracture strain of longitudinal reinforcement	ε_u	0.18	-
Ultimate strength of reinforcement	f_u	620	-
Strain at maximum stress of transverse reinforcement	ε_r	0.15	-
Compressive strength of concrete	f_c	35	MPa
Strain at maximum stress of concrete	ε_0	0.002	-
Axial compressive load on each column	N_u	280	kN

Table 3. Estimated mas loss percentages

Frame	t_p	ψ_{tc}	ψ_{tb}	ψ_{lc}	ψ_{lb}
Frame A	0	0	0	0	0
Frame B	10	10.87	10.87	4.15	4.61
Frame C	40	27.7	27.7	10.91	12.1
Frame D	100	49.15	49.15	20.36	22.48

Time from corrosion initiation (t_p), mass loss percentage of transverse reinforcements of column (ψ_{tc}), mass loss percentage of transverse reinforcements of beam (ψ_{tb}), mass loss percentage of longitudinal reinforcements of column (ψ_{lc}), mass loss percentage of longitudinal reinforcements of beam (ψ_{lb})

3. Proposed NFE model of hypothetical RC frame

In this study, to simulate the nonlinear structural response of the hypothetical RC frame, an advanced fibre-based modelling strategy is adopted. Figure 3 shows the proposed NFE model of the considered RC frame. As Figure 3 shows, each column is divided into two force-based elements (Force-Based Element C1 and Force-Based Element C2). These two elements are discretised to several fibre-sections at integration points. The beam element is composed of three force-based elements. At beam-column connection regions, as well as the column footings, zero-length section element is used to account for the reinforcement slippage (Zhao & Sritharan, 2007). The accuracy of the proposed modelling strategy is validated against experimental results in the authors' previous studies (Dizaj et al., 2018a; Kashani et al., 2016). Further details about the proposed NFE model are provided in (Dizaj et al., 2018b). It worth noting that, the nonlinear finite element model presented in Figure 3 can model different mass loss percentages for each element and each fibre section. However, the results presented in (Dizaj et al., 2018b) showed that the record-to-record variability of ground motions have a much more significant impact than spatial variability of pitting corrosion on the nonlinear dynamic behaviour and fragility of corrosion-damaged RC frames. Therefore, the main focus of the current study is on the impact of main-shock aftershock sequences.

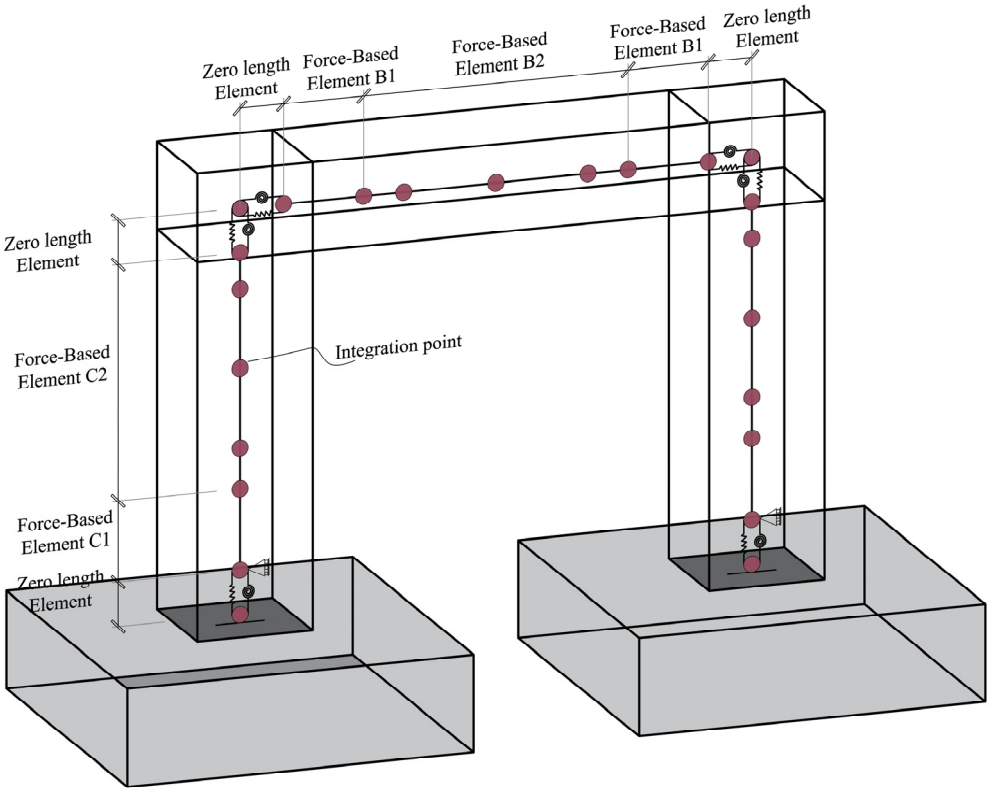

Figure 3. Proposed NFE model of RC frames

The stress-strain behaviour of reinforcing steel bars is modelled by the phenomenological constitutive material model developed by Kashani et al. (2015a). This model simulates the negative influence of corrosion damage on inelastic buckling and fatigue degradation of reinforcing bars. According to this model, the mechanical properties of corroded reinforcement should be modified based on the empirical equations proposed by Du et al. (2005a, 2005b):

$$f_y^{corr} = (1 - 0.005\psi) f_y \tag{2}$$

$$\varepsilon_u^{corr} = (1 - 0.05\psi)\, \varepsilon_u \tag{3}$$

where f_y^{corr} and ε_u^{corr} are yield strength and fracture strain of corroded reinforcement, and f_y and ε_u are yield strength and fracture strain of uncorroded reinforcement. The post-yield buckling response of the corroded reinforcing bars is characterised using an exponential function. Further details on the employed buckling model are available in (Kashani et al., 2015a).

To take into account the effects of low-cycle fatigue degradation of reinforcing bars, the generic *Fatigue* model, available in the OpenSees as *UniaxialMaterial Fatigue* (Uriz, 2005), is wrapped to parent phenomenological material model of reinforcing steel bars. To describe the low-cycle fatigue failure (Manson, 1965; Miner, 1945), this material model employs Coffin– Manson relationship and Miner's rule:

$$\varepsilon_p = \Phi(2N_f)^{-\alpha} \tag{4}$$

where α and Φ are the material constants, ε_p is the amplitude of plastic strain, and $2N_f$ is the number of half-cycles to failure. To take into account the influence of inelastic buckling on fatigue life of reinforcing bars, in this study, the material constant parameters α and Φ are chosen to be -0.393 and 0.138 (Kashani et al., 2015b). To capture the adverse impact of corrosion on fatigue life of reinforcement, Kashani et al. (2015a) proposed the following empirical relationship between mass loss percentage (ψ) and material constant α:

$$\alpha_{corr} = (1 + 0.004\psi)\alpha \tag{5}$$

where α_{corr} is the material constant for corrosion damaged reinforcement. The *Fatigue* material represents the state of low-cycle fatigue degradation of reinforcement as a fatigue damage index which is an integer between 0 and 1. Once the fatigue damage index reaches 1, the stress of the parent longitudinal reinforcement material model becomes zero. Figure 4 displays the simulated nonlinear behaviour of reinforcing steel bars in tension and compression.

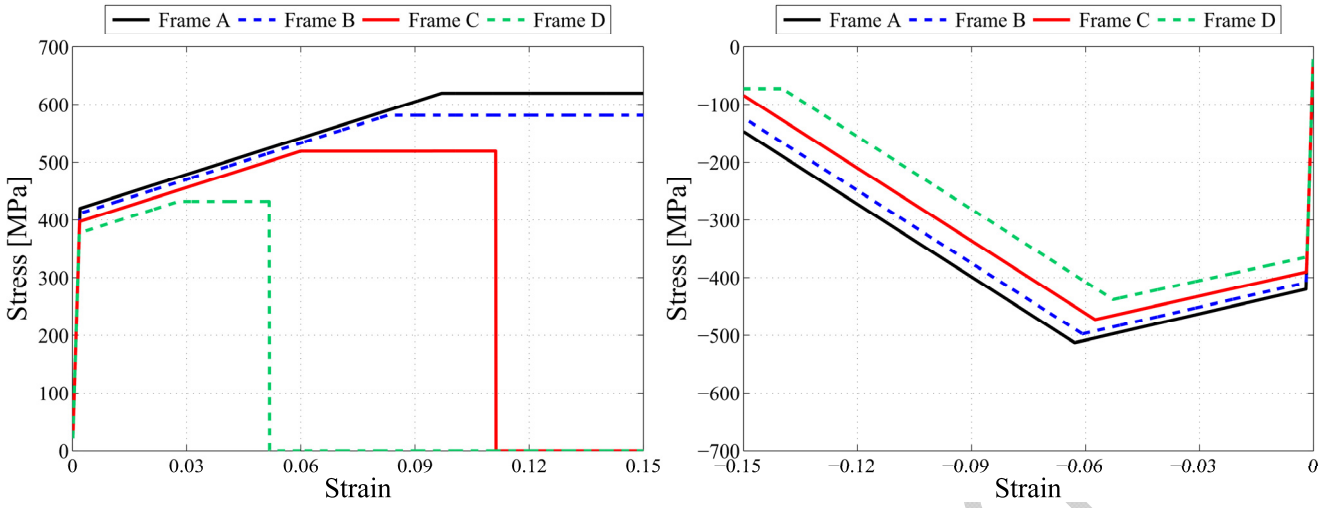

Figure 4. Simulated stress-strain behaviour of reinforcing bars: (a) tensile behaviour, and (b) compressive behaviour

The nonlinear stress-strain behaviour of concrete material is defined by Kent-Scot-Park (Scott et al., 1982) concrete model with a bilinear tension response and a parabolic compression response. This material is defined using *Concrete 02* material model available in OpenSees (McKenna, 2011). The ultimate compressive strain of pristine unconfined concrete (concrete cover), $\varepsilon_{u,cover}$ is limited to 0.004 (Priestley & Paulay, 1992).

The accumulation of corrosion products around the reinforcement, however, leads to corrosion-induced concrete cover cracking. To capture this phenomenon, in numerical modelling the compressive strength and ultimate compressive strain of concrete cover should be modified. Therefore, for corroded case-study structures, both f_c and $\varepsilon_{u,cover}$ are modified based on the methodology proposed in (Coronelli & Gambarova, 2004). According to this methodology, for corroded RC sections, f_c should be reduced by the reduction factor γ, where γ should be calculated using Equation (6):

$$\gamma = \frac{1}{1 + \dfrac{\pi\, n\, D \left[\rho_{rust} - 1\right]\left[1 - 0.1\sqrt{100 - \psi}\right]}{10\, B\, \varepsilon_0}} \tag{6}$$

where n is the number of compressive bars of the column/beam section, ρ_{rust} is the ratio of volumetric expansion of corrosion products to uncorroded steel which can be taken as 2, B is the column/beam width, and D is the bar diameter of uncorroded longitudinal reinforcement. For the proposed RC frame of this study, the longitudinal bar diameters of columns and beam are 20 mm and 18 mm, respectively. In relation to the pristine confined concrete, the positive influence of confinement on maximum compressive stress (σ_{cc}) and ultimate strain ($\varepsilon_{u,core}$) is considered according to Equations (7-8) (Priestley and Paulay, 1992; Scott et al., 1982;):

$$f_{cc} = \left(1 + \frac{\rho_t f_{yh}}{f_c}\right) f_c \tag{7}$$

$$\varepsilon_{u,core} = 0.004 + 1.4\left(\frac{\rho_t f_{yh} \varepsilon_r}{f_{cc}}\right) \tag{8}$$

where ρ_t is the volumetric ratio of transverse reinforcement. However, as the corrosion level increases, the volumetric ratio of confinement significantly decreases. This results in premature fracture of confinement and as a result, premature confined concrete crushing. To account for the negative influence of corrosion, for corroded frames, f_{cc} and $\varepsilon_{u,core}$ are modified based on a simplified methodology presented in (Dizaj et al., 2018a). According to this methodology, for corroded frames, ρ_t, f_{yh} and ε_r should be replaced by ρ_t^{corr}, f_{yh}^{corr} and ε_r^{corr}:

$$\rho_t^{corr} = \left(1 - 0.01\psi_t\right)\rho_t \tag{9}$$

$$f_{yh}^{corr} = \left(1 - 0.005\psi_t\right) f_{yh} \tag{10}$$

$$\varepsilon_r^{corr} = \left(1 - 0.05\psi_t\right)\varepsilon_r \tag{11}$$

where ψ_t is the mass loss percentage of transverse reinforcement. It should be noted that alternative models have also been proposed for the ductility reduction of the corroded reinforcing bars (e.g the model

proposed by Apostolopoulos and Papadakis (2008)). However, Equation (3) proposed by Du et al. (2005b), has been widely used in the literature; and hence, this model is employed here to modify ε_r.

In Table 4, the modified values of f_c, f_{cc}, $\varepsilon_{u,cover}$ and $\varepsilon_{u,core}$ for either pristine or corroded hypothetical frames are presented.

Table 4. Modified compressive properties of concrete material

Frame	t_p	f_c [MPa]	f_{cc} [MPa]	$\varepsilon_{u,cover}$	$\varepsilon_{u,core}$
Frame A	0	35	41.28	0.0040	0.0360
Frame B	10	23.4	40.29	0.0027	0.0211
Frame C	40	15.1	38.91	0.0017	0.0046
Frame D	100	9.9	37.41	0.0011	0.0040

The bond-slip degradation at the column-footing interface and beam-column connection regions is considered using nonlinear zero length section elements (Dizaj et al., 2018b). At the column-footing interface, the uncorroded bond-slip model proposed by Zhao and Sritharan (2007) is used as it is unlikely that they are corroded in that depth. At the beam-column connection, a simple procedure is employed to account for the bond-slip deterioration due to the corrosion. Further details are available in Dizaj et al. (2018b).

4. Quantification of corrosion-variant DLS

The seismic vulnerability assessment of structures is normally carried out by adopting several specific DLS criteria. In literature, the original DLS definitions provided in HAZUS-MR5 (2010) have been widely used by researchers to conduct reliability and seismic vulnerability assessments (Alipour et al., 2011; Cui et al., 2018). These DLS, however, do not account for material ageing and time-dependent structural degradation. The inappropriateness of time-independent DLS in vulnerability assessment of corrosion-damaged RC structures is demonstrated in (Dizaj et al., 2018a). In this study, the DLSs are defined based on the methodology proposed in (Dizaj et al., 2018b). On this basis, the moderate DLS is

considered to be the drift at first yielding of longitudinal bars; the extensive DLS is considered to be the drift at spalling of concrete cover, and the complete collapse is considered to be the associated drift with confined concrete failure (crushing) or first fracture of longitudinal reinforcing bars (each one takes place earlier). In this way, the DLS will be a corrosion-variant parameter (Dizaj et al., 2018b).

To quantify the defined Corrosion-dependent Damage Limit States (CDLS), monotonic pushover analysis conducted on each frame. Both of the columns are considered to be fully fixed at their base connection. The mass of the structure is modelled as a lumped mass on top of each column. The P-Δ effects caused by axial compressive load on each column (defined in Table 2) is considered in the analyses using P-Δ transformation (available in OpenSees). Moreover, the material responses are recorded during the analysis.

Figure 5 shows the results of pushover analysis. The defined DLSs are shown on the normalised base shear-drift response of each frame. The normalised base shear is the base shear of each frame divided by the maximum base shear of frame A. As Figure 5 indicates, the defined moderate and extensive DLS criteria for the pristine frame (Frame A) are associated with approximately 1% and 3% drifts, respectively, and therefore, are in line with those proposed in HAZUS MR5 (2010). For frame A and B, the associated drift of complete collapse DLS is kept as 0.08. Figure 5 indicates that the DLSs of corroded frames take place in lower drifts in comparison with those of pristine frame. Moreover, the ductility and strength of frames decrease significantly as the corrosion level increases. The extracted DLSs from Figure 5, will be implemented in section 6.3 to develop corrosion-variant MS and MS-AS fragility curves.

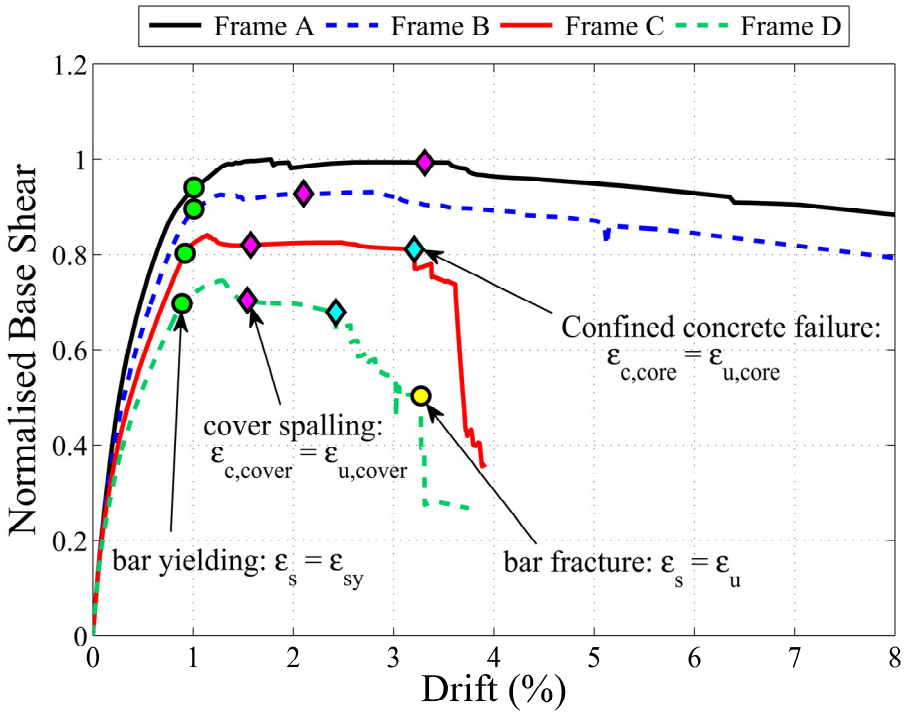

Figure 5. Pushover analyses results

5. MS-AS ground motion selection

The selection of aftershocks is an important task in seismic performance and vulnerability assessment of structures, as it directly influences the outcomes and results of any investigation. It has been a common practice to use artificial sequences mainly using the back-to-back method, in which the mainshock is scalded and used as an aftershock (Li & Ellingwood, 2007; Ryu et al., 2011). However, it has been established that not carefully selected mainshock-aftershock (MS-AS) records may impose a significant bias in the structural response prediction (Goda, 2015). Recently, the application of real as-recorded MS-AS ground motion records has gained attention due to available online ground motion databases such as Pacific Earthquake Engineering Research-Next Generation Attenuation (PEER-NGA) and Japanese databases such as the Kyoshin and Kiban-Kyoshin networks (K-NET/KiK-net).Examples can be found in Goda and Taylor (2012), Goda and Salami (2014), Ebrahimian et al. (2014) and Salami et al. (2019).

Likewise, in this paper, real MSAS ground motions have been selected to conduct the IDA of pristine and corroded RC frames.

To incorporate the local seismicity and hazard level of a site, it was assumed that the frame is located in Riverside, California (latitude/longitude = 33.979/-177.335). The soil is assumed to be of the NEHRP soil C classification (Vs=537 m/s). The Uniform Hazard Spectrum (UHS) curve with a 2% probability of exceedance in 50 years for the site is provided by the U.S. Geological Survey (https://www.usgs.gov), as presented in Figure 6(a). The Intensity Measure (IM) selected in this paper is 5% damped spectral acceleration response at the building's estimated first mode period Sa(T_1) where T_1 is the first natural vibration period of the frame and it is equal to 0.44 seconds. It should be notified that the calculated fundamental period (T_1) in OpenSees is based on the un-cracked stiffness of the members, where damage in steel has almost no impact on the natural frequency/period of the structure; the biggest impact comes from concrete cracking/spalling (Ge et al., 2020; Kashani et al., 2019). Therefore, T_1=0.44 seconds has been adopted as the first natural vibration period of all the considered frames with different corrosion degrees.

In addition to the UHS curve, the predicted median spectrums generated by the Ground Motion Prediction Equations (GMPEs) proposed by USGS are also presented in Figure 6(a). The average predicted median spectrum and $+\varepsilon\sigma$ spectrum associated with M=7.03, R=10.39 km, and ε=1.6 from GMPEs are also presented. The mean values for magnitude and distance are taken from the disaggregation information for the specific location, extracted from the Probabilistic Hazard Analysis (PSHA) provided by USGS. The disaggregation data for the site is presented in Figure 6(b). The ground motion records for this study, are limited to crustal shallow earthquakes more suitable for tectonic characteristics of California, US. Therefore, records with a distance of more than 40 km are filtered out from the database. Having the disaggregation information (average values of distance and magnitude),

and the predicted median spectrum from GMPEs, a single target response spectrum (CMS) can be constructed to select the records suitable for the specific location and building information (Baker, 2011).

After defining the target CMS, presented in Figure 6(c) ground motion sequences are selected for time-history analysis. To have a sufficient number of records and compensate for the lack of locally recorded ground motion sequences, a combined MS-AS database based on the K-NET/KiK-net database for Japanese earthquakes (Goda, 2012) and PEER-NGA database for worldwide shallow crustal earthquakes (Goda & Taylor, 2012) is utilised. The database contains 290 MSAS sequences (two horizontal components per sequence). Their response spectrum and the CMS target are presented in Figure 6(c). The selection procedure is based on calculating the error using the Sum of Squared Errors (SSE) in logarithmic space between the geometric mean of two horizontal components and the target CMS. The error calculation is conducted on the sensitive period range of the structure and it is taken to be between $0.2T_1$ and $2.0T_1$ as it was recommended by Vamvatsikos and Cornell (2005) and Baker and Cornell (2008). The period range for selection and the selected records are presented in Figure 6(d). In total, 24 ground motion records (i.e. the geometric mean of two horizontal components) extracted from the database that provides 48 MS-AS records to be utilised in IDAs. The summary of the constructed real MS-AS ground motion sequences has been added in Appendix A of the paper to provide more information.

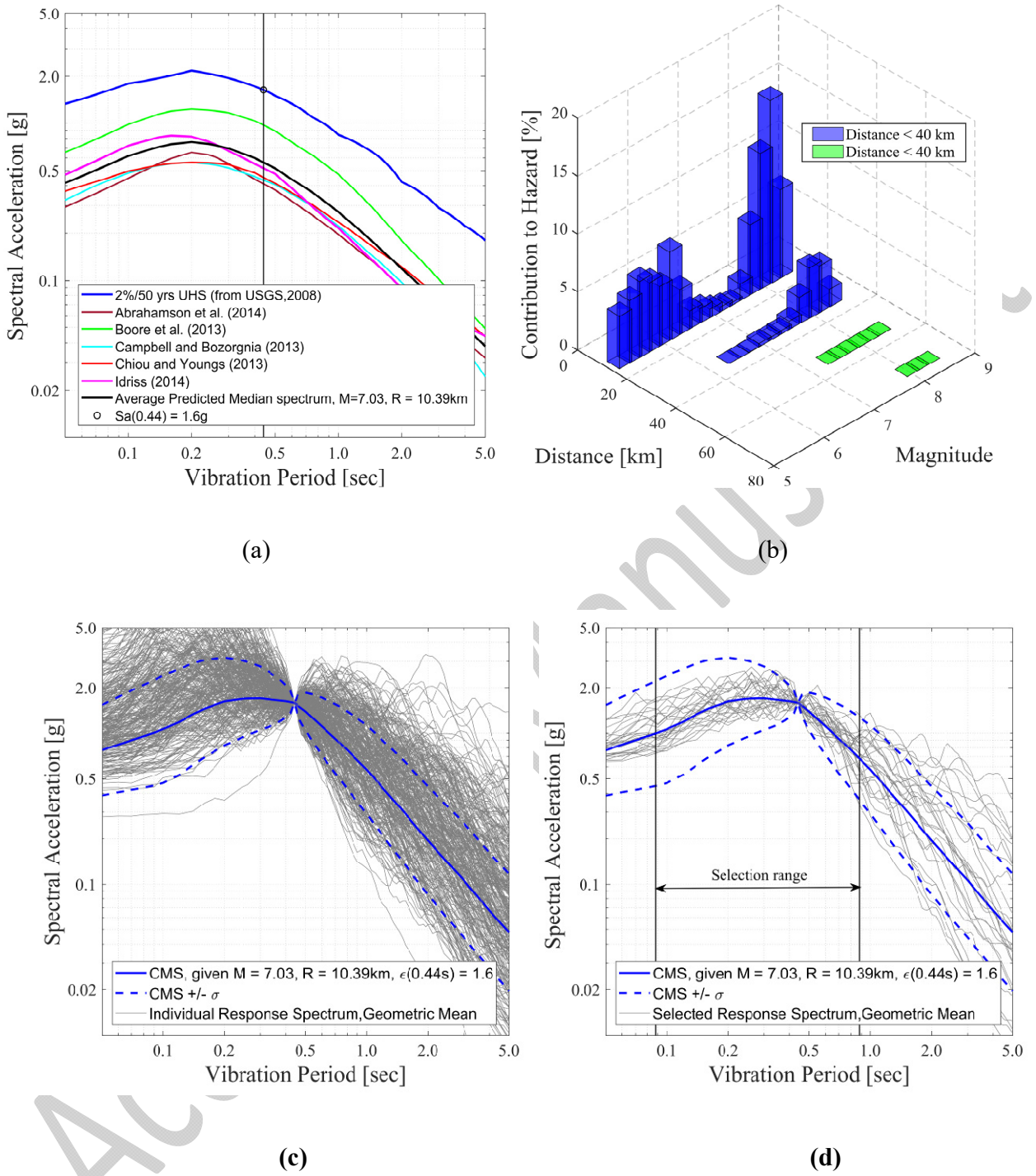

Figure 6. Ground motions selection, (a) UHS for Riverside, California with GMPEs and average predicted median spectrum, (b) disaggregation information from USGH, (c) CMS with the geometric mean of all individual ground motions, (d) selected records ready to use in IDAs.

6. Results and discussions

6.1 MS versus MS-AS IDA results

IDA method is an effective tool to study the nonlinear dynamic response of structures, as it tracks the overall behaviour of structures from minor damage to complete collapse (Vamvatsikos, 2002). To investigate the nonlinear dynamic response of the hypothetical frames, the selected MS-AS ground motion pairs are applied to the hypothetical frames with a wide range of increasing intensity levels. Here, the first-mode spectral acceleration response ($Sa(T_1, 5\%)$) is considered as IM, and drift (roof displacement divided by column height) considered as Damage Measure (DM).

To conduct IDAs, first between each MS and its subsequent AS a Time Gap (TG) of 60 seconds with zero accelerations is inserted. Then, the whole continuous series of MS-TG-AS accelerations are applied to the structures as a single ground motion input. Figure 7 shows an exemplar acceleration time series of the selected MS-AS ground motion records. During each analysis, the structural response (drift, material responses, etc) are recorded continuously from the beginning to the end; therefore, the analyses outputs under MS can be extracted and compared with those under MS-AS sequence.

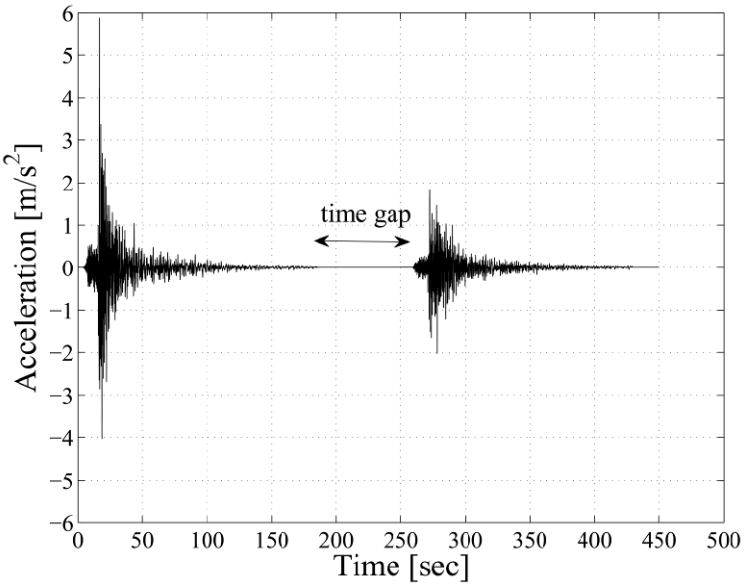

Figure 7. An example of selected MS-AS sequence

Figure 8 shows individual and summarised IDA results for each hypothetical frame. Figure 8 shows that for approximately less than 0.03 drift ratio the median IDA curve of MS-AS coincides that of MS. However, beyond this range, for a specific IM, frames subject to MS-AS sequence experience higher drifts comparing to those subject to MS. For example, while for IM=4g the peak drift ratio of frame A is less than 0.06; under MS-AS sequence and same IM, it is approximately 0.075 (Figure 8(a)). It can be seen a similar trend in Figure 7(b) for the slightly corroded frame (frame B). However, as Figures 8(c) and 8(d) indicate the median IDA curves of frame C and frame D under MS-AS sequence are much close to those under MS. More specifically, for the severely corroded frame (Frame D) the median responses of the structure under MS and MS-AS are approximately the same. This is because, the higher corrosion levels lead to premature material failure (as it will be discussed in the next section); and as a result, the structure collapses under the first event (i.e. MS) before the second event taking place. This finding is in a good agreement with results of shake table tests on corroded RC columns (Ge et al., 2020; Kashani et al., 2019).

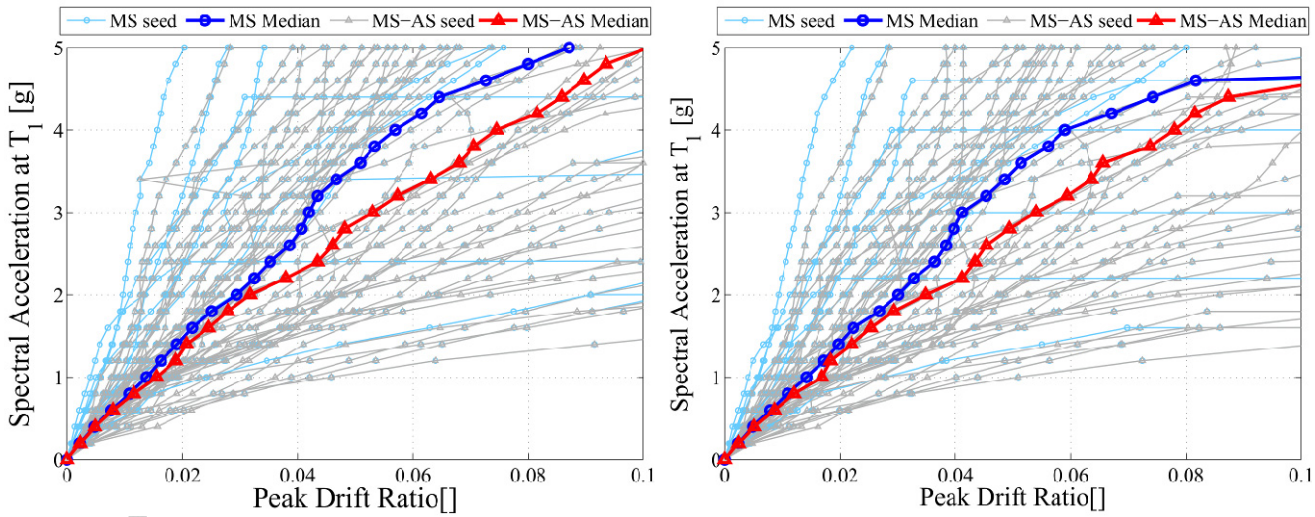

(a) **(b)**

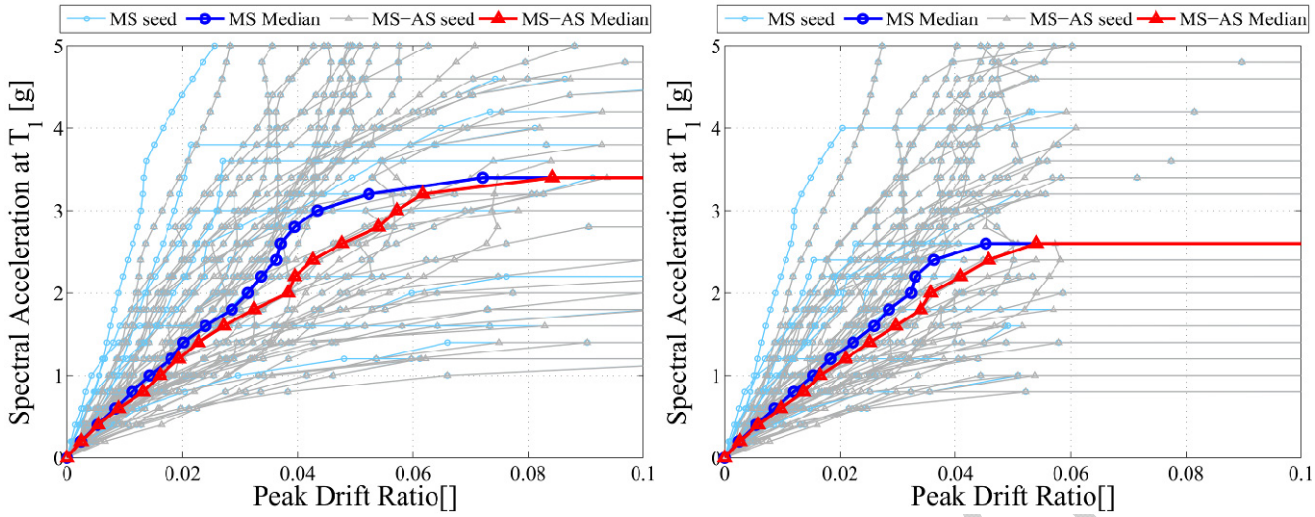

Figure 8. MS versus MS-AS IDA outputs: (a) Frame A; (b) Frame B; (c) Frame C, and (d) Frame D

6.2 Damage evaluation at the material scale

The former section depicted the global behaviour of the considered structures under MS event and MS-AS sequence. It was shown that there is no significant difference between the overall response of highly corroded frames (frame C and frame D) under MS-AS sequence and single MS event. To investigate why such behaviour takes place, the material response of concrete and all the steel bars are recorded at the base of columns for each IDA under MS for further investigation. The progression of three common sources of material failures, such as concrete crushing, rebar fracture and fatigue failure is tracked for each input intensity level. To make these three damage types comparable, the maximum compressive strain of confined concrete $(\varepsilon_{c,core})_{max}$ (considering both the left and right columns) at each input IM is divided by its ultimate strain $(\varepsilon_{u,core})$ to get Normalised Confined Concrete (Norm. CC) strain. Similarly, to have Normalised Steel tensile strain of Steel reinforcements (Norm. S strain), the maximum tensile strain of all the longitudinal reinforcements under each IM is normalised by the fracture strain (ε_u). In this way, the amount of both the Norm. CC and Norm. S strain values will be between 0 and 1, and

therefore, will be comparable with the fatigue damage index (Kashani et al., 2015a, 2017) of reinforcements.

As it is shown in Figure 5, the confined concrete crushing is the dominant failure mode of all the studied frames. On this basis, to explore the state of other damage types at the onset of concrete crushing, the associated Norm S strain, fatigue index, and drift ratio to $(\varepsilon_{c,core})_{\max}$ are extracted and plotted in Figure 9. Figure 9 indicates that, while in frame A and frame B, the indices of all the three damage types are less than 0.2 (Figures 9(a-b)); in frames C and D the confined concrete crushing is the predominant damage mechanism and takes place in relatively small drift ratios (Figures 9(c-d)). For example, as can be seen in Figure 9(d), even in less than 0.01 drift ratio frame D fails due to premature confined concrete crushing. This implies that, as corrosion level increases, the failure is mainly occurring in the core confined concrete. This is because, as corrosion level increases, the cross-sectional area of confining reinforcement significantly decreases; and therefore, the premature fracture of confinement results in premature crushing of core confined concrete. Therefore, it can be concluded that, under the stronger shock (here the MS), the severely corroded RC structures are likely to fail before the second event comes up. This will be further discussed in section 6.4.

In Figure 9, the DLSs extracted from pushover analyses (section 4) are shown with vertical solid lines to compare them with the state of different sources of material damage under IDAs. Figure 9(c) and Figure 9(d) show that the adopted complete collapse limit state (complete DLS) is a relatively good indicator of the onset of core concrete crushing. Moreover, Figure 9 shows that under the time-history analyses the fatigue failure of reinforcement is not critical; and therefore, the adopted DLSs are appropriate criteria to develop the fragility curves.

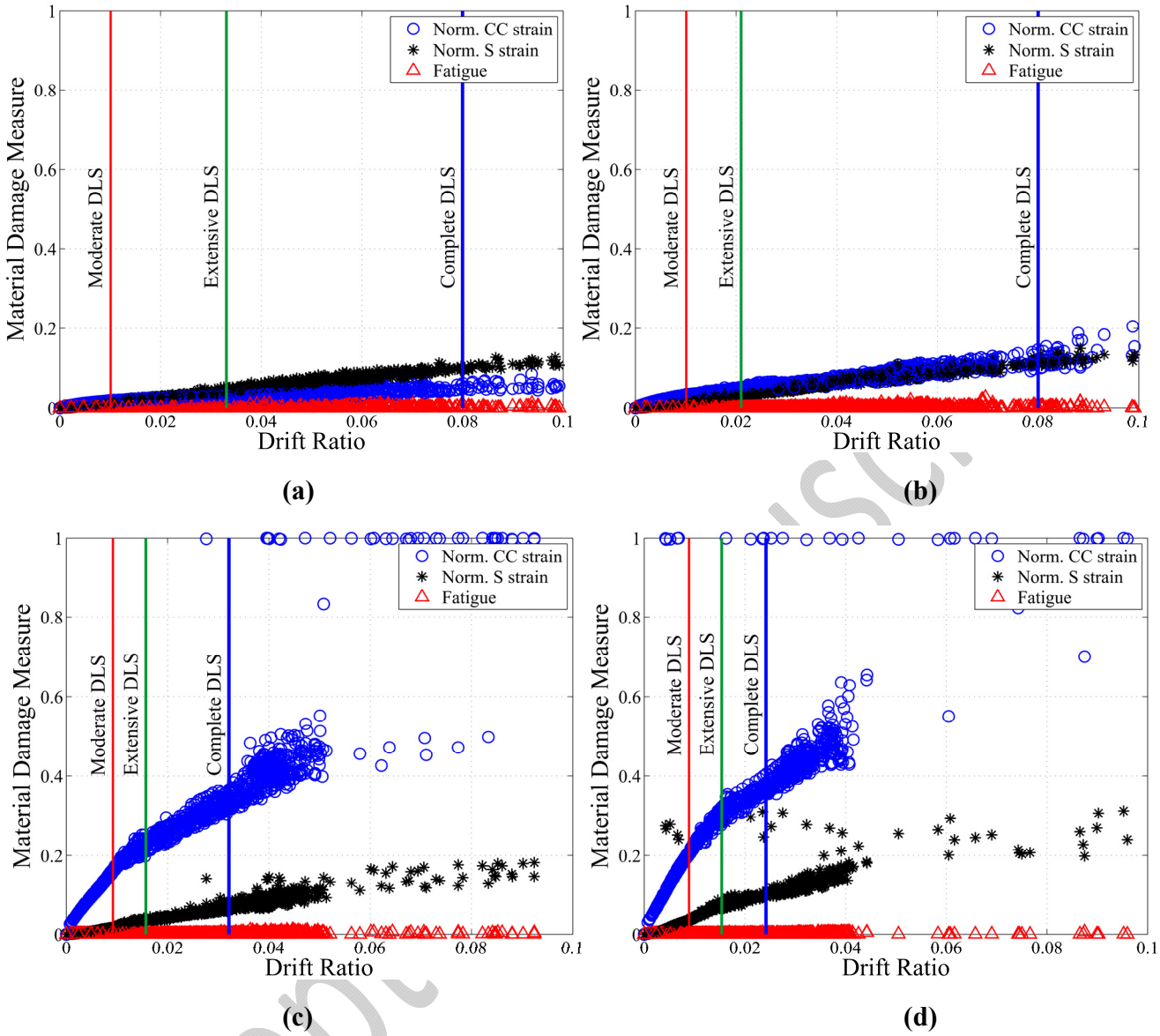

Figure 9. Comparing damage indicators at the material scale under MS event: (a) Frame A; (b) Frame B; (c) Frame C, and (d) Frame D

6.3 MS and MS-AS fragility assessment

In this section, using the IDA outputs fragility curves are developed for each frame based on the corrosion-variant DLSs obtained in section 4. To this aim, from the IDA results, firstly Peak Drift Ratios (PDRs) corresponding to each Intensity Measure (IM) of each ground motion (here, IM=Sa (T_1)) are extracted. Subsequently, using the following fragility function, the probability of exceeding moderate DLS, extensive DLS and complete DLS of each frame is calculated to develop the fragility curves:

$$P\left[PDR \geq DLS \mid IM = x\right] = 1 - \Phi\left(\frac{\ln(\mathrm{DLS}) - \ln(\mu)}{\beta}\right) \tag{12}$$

where P[.] is the probability that PDR exceeds the DLS given that the IM of input event is *x*. It has been widely accepted that PDRs for a given IM (i.e. Sa (T_1)) follow a lognormal distribution ($\Phi(.)$) with the logarithmic mean value of $\ln(\mu)$ and logarithmic standard deviation value of β (Salami et al. 2019):

$$\ln(\mu) = \frac{\sum_{i=1}^{n} \ln(\mathrm{PDR}_i)}{n} \tag{13}$$

$$\beta = \sqrt{\frac{\sum_{i=1}^{n} \left(\ln(\mathrm{PDR}_i) - \ln(\mu)\right)^2}{n-1}} \tag{14}$$

where *n* is the number of ground motions, and PDR_i is the value of PDR corresponding to a given IM for the *i*th ground motion.

Figure 10 shows the MS versus MS-AS fragility curves for each frame. As can be seen in Figure 10, for individual hypothetical frames and at a given IM, the collapse probability of each frame under MS-AS sequence is slightly higher than MS earthquake. For frame C, as an example, the probability of exceeding complete DLS under MS-AS is approximately 7% higher than MS. A similar trend can be seen for moderate and extensive DLSs. Overall, similar to the observed IDA results (Figure 8), this slight difference is negligible. This might be due to the nature of selected MS-AS sequences. This is further discussed in more details in section 6.4.

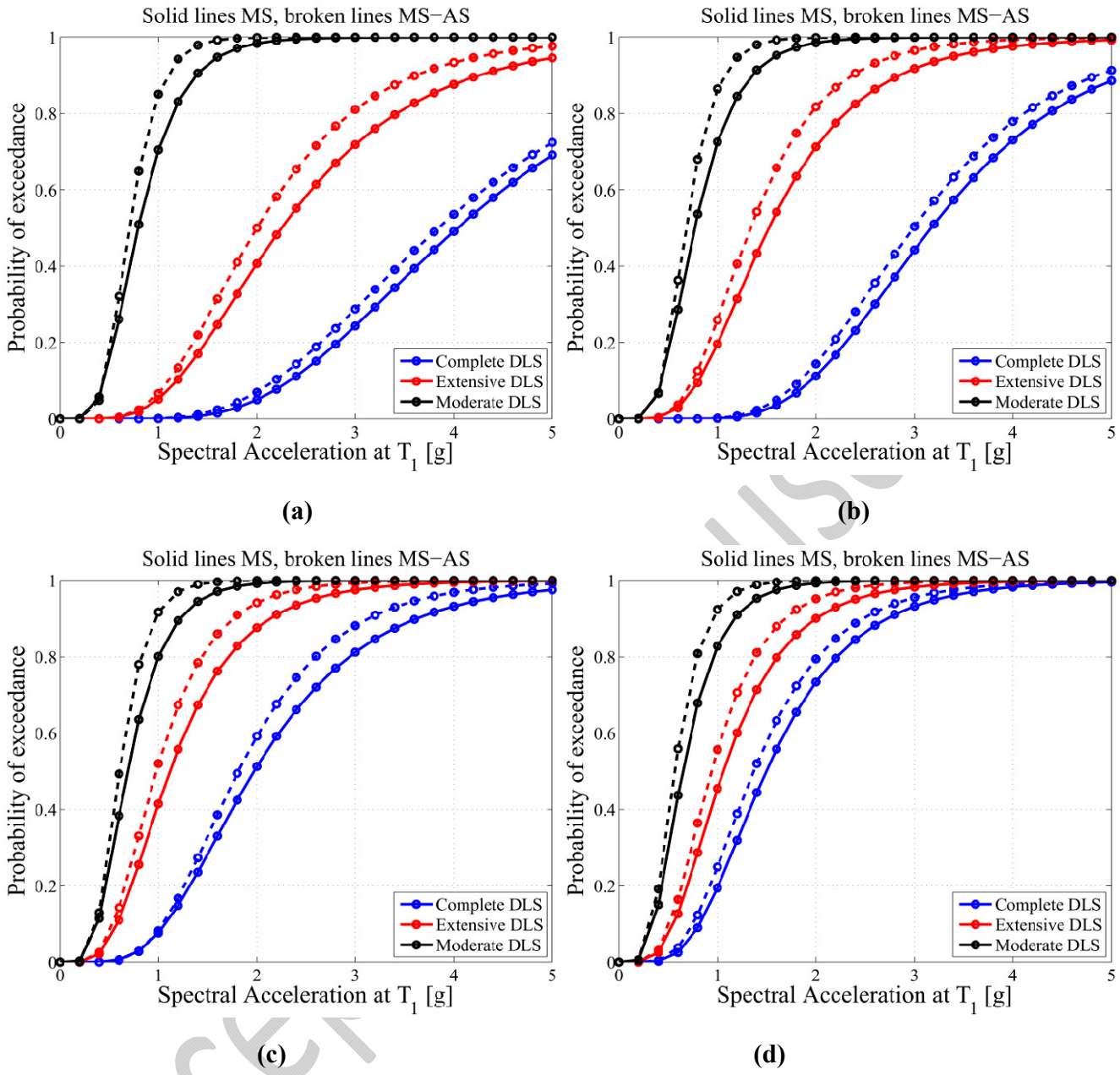

Figure 10. MS versus MS-AS fragility curves: (a) Frame A; (b) Frame B; (c) Frame C, and (d) Frame D

6.4 Effect of AS to MS PGA ratio

In the previous section, it was shown that the occurrence of a second successive event (AS) has a negligible impact on the median nonlinear dynamic behaviour and collapse probability of considered frames (especially those with higher degrees of corrosion). However, one reason for such behaviour

might be related to lower overall intensity level of the second event (i.e. AS) in comparison with the first event (i.e. MS).

The current section highlights this matter. To this purpose, first, the intensity of AS is compared with MS in term of PGA. Figure 11, shows PGA ratio of the AS to MS (PGA_{AS}/PGA_{MS}) for all the selected ground motion records. As can be seen in Figure 11, just in 8 ground motions (out of 48 ground motions) the PGA ratio of AS to MS is higher than 1. Details of these 8 ground motions are available in Table A1 (in Appendix A) of the current paper. Therefore, to investigate the impact of PGA ratio of AS to MS on nonlinear behaviour and fragility of considered frames, the IDA results under these 8 ground motions are extracted and plotted separately in Figure 12. As Figure 12 indicates, for PGA_{AS}/PGA_{MS} >1 ground motion pairs, the AS aggravates significantly the global damage indicator (drift ratio) in all the frames. For example, while for IM=2g the peak drift ratio of frame C under MS is approximately 0.02; It reaches to around 0.046 under corresponding MS-AS (Figure 12(c)). Such behaviour can also be seen in Frames A, B and D.

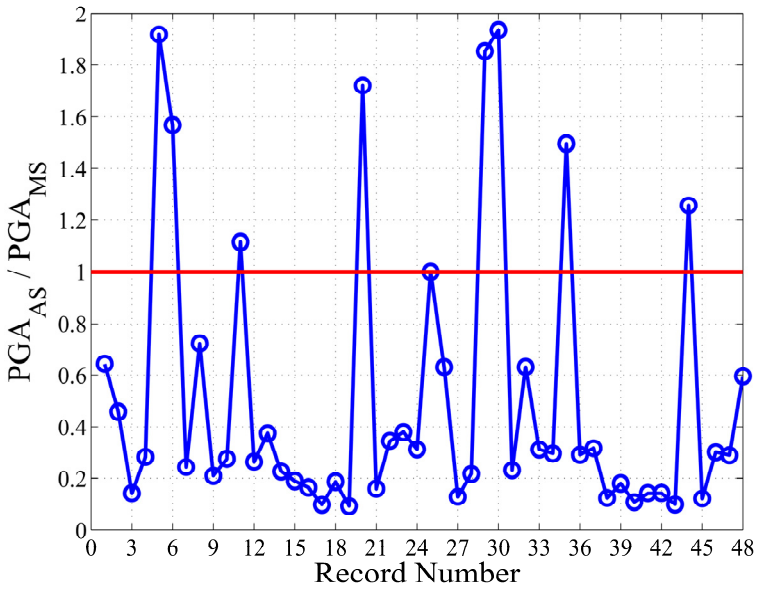

Figure 11. AS to MS PGA ratio for selected ground motion records

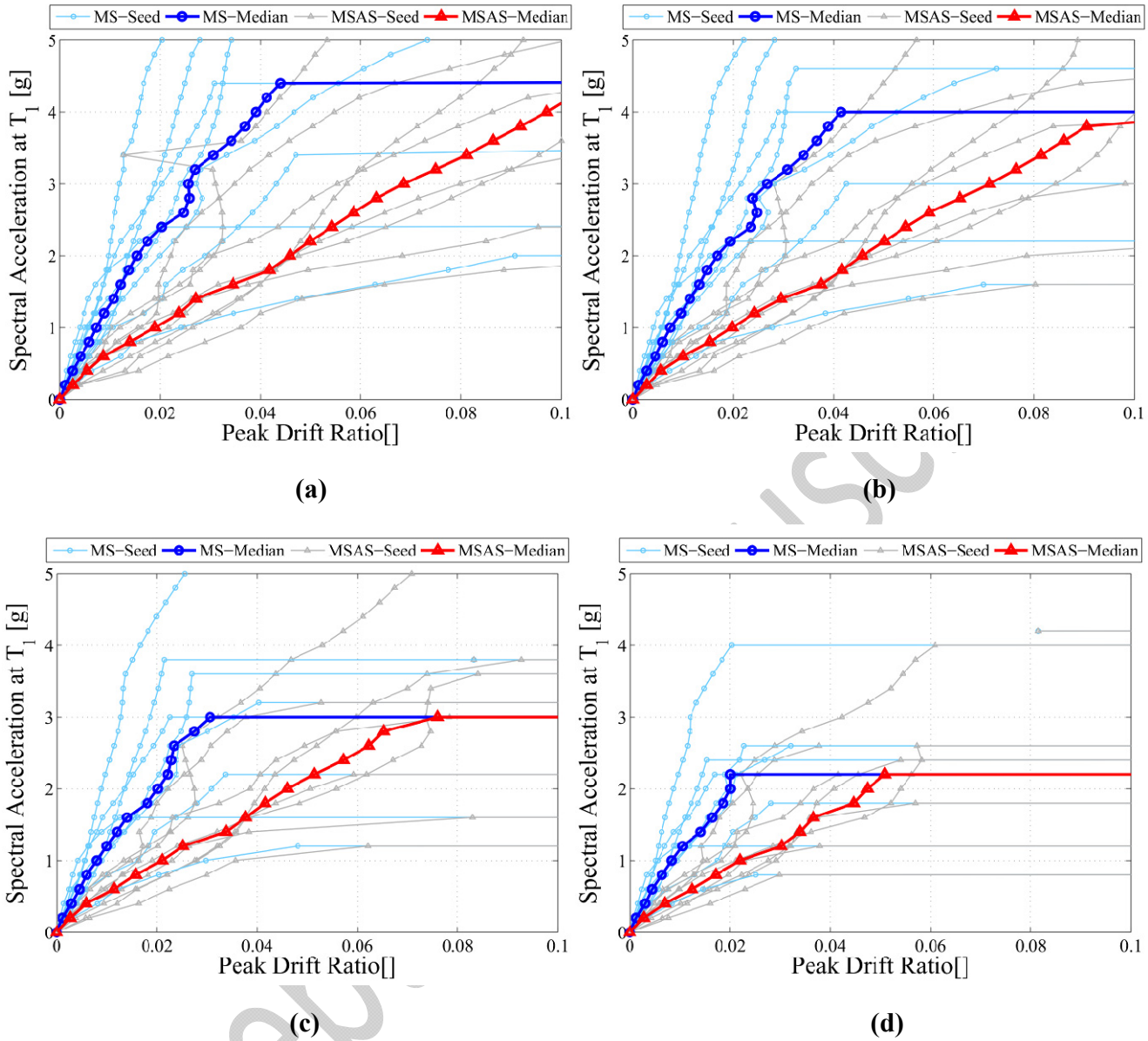

Figure 12. MS versus MS-AS IDA outputs for records with $PGA_{AS}/PGA_{MS}>1$: (a) Frame A; (b) Frame B; (c) Frame C, and (d) Frame D

To investigate the impact of PGA ratio of AS to MS on the failure probability of the hypothetical frames, using the IDA outputs under $PGA_{AS}/PGA_{MS}>1$ record pairs (Figure 12), the collapse fragility of the frames are plotted in Figure 13 using the same procedure described in section 6.3. Figure 13 shows that the probability of collapse of the pristine frame and the slightly corroded frame is not significantly affected by PGA ratio of AS to MS (Figure 13(a-b)). In other words, as it was shown in Figure 10(a-b), the influence of AS event on collapse probability of frame A and frame B is negligible. However, it can

be seen from Figure 13(c-d) that under $PGA_{AS}/PGA_{MS}>1$ record pairs the moderately and severely corroded frames are much more vulnerable than those subject to $PGA_{AS}/PGA_{MS}<1$ ground motions (Figure 10(c-d)). For example, for IM=2g, the collapse probability of frame C and frame D under $PGA_{AS}/PGA_{MS}>1$ MS-AS sequences is increased by approximately 50% and 35%, respectively compared to MS event. This demonstrates that the PGA ratio of AS to MS plays a key role in fragility assessment of corroded RC frames.

It should be noted that in the current study the effect PGA_{AS}/PGA_{MS} is investigated using a limited number of ground motion pairs (8 records). This is an area for further research.

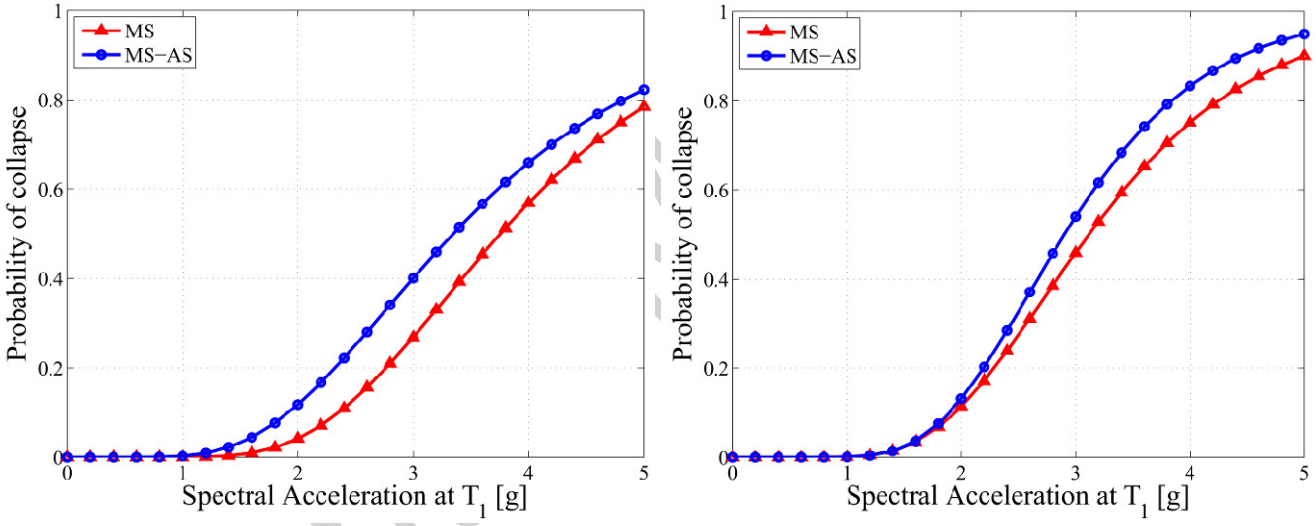

(a) **(b)**

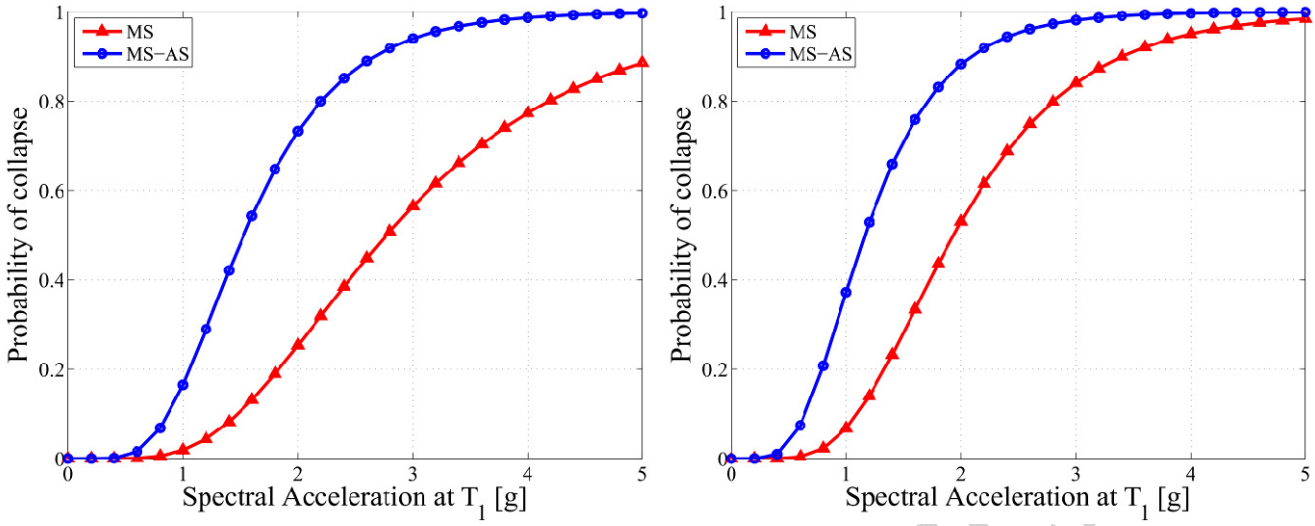

(c) **(d)**

Figure 13. Collapse fragility curves for records with $PGA_{AS}/PGA_{MS}>1$: (a) Frame A; (b) Frame B; (c) Frame C, and (d) Frame D

7. Conclusion

In this study, a framework is proposed for fragility analysis of deteriorated RC frames subject to real MS-AS ground motions. Firstly, corrosion-variant pushover analyses conducted on a case-study RC frame with various corrosion damage levels to quantify the corrosion-variant DLS. Then, IDAs were conducted on the considered frames using 48 real MS-AS sequences; and then, damage mechanisms and failure probability of case-study structures under MS events and MS-AS sequences analysed. Finally, the impact of the PGA ratio of AS to MS in vulnerability assessment of case-study structures was investigated.

The following are the key conclusions of this study:

- The median IM-DM IDA response of severely corroded frame under MS events and MS-AS sequences are approximately the same. This can be attributed to the premature material failure of the frame under the first event (i.e. MS) which results in brittle collapses of the structure.

- As corrosion level increases, due to the significant reduction in cross-sectional area of confining reinforcement, the damage/failure is mainly accumulated in confined concrete. This is the main reason for the brittle collapse of severely corroded RC structures under the single MS excitations.
- The collapse probability of the studied frames is slightly higher under the MS-AS sequences. For example, under MS-AS event, the probability of failure of Frame C is approximately 7% higher than MS.
- In PGA_{AS}/PGA_{MS} >1 ground motion pairs, the AS significantly intensifies the drift ratio of all the considered frames. For example, under IM=3g, the median maximum drift ratio of frame C under MS-AS sequences is approximately equal to 2.5 times the median maximum drift ratio of this frame under MS event.
- While PGA ratio of AS to MS does not affect the collapse probability of pristine frame and slightly corroded frame, it significantly influences the fragility estimation of moderately and severely corroded frames. For example, PGA_{AS}/PGA_{MS}>1 ground motions, increase the collapse probability of frame C and frame D by approximately 55% and 35%, respectively comparing to MS event. This demonstrates that the PGA ratio of AS to MS plays a key role in vulnerability assessment of corroded RC frames.

It should be noted that the findings of the current study are valid for the selected site-specific ground motions, and the case-study structure used in this paper. Therefore, the research outcome of this study may not be generalised for a different class of corroded structures and ground motions types. Nevertheless, this study provides an insight and platform for future research to other researchers in modelling nonlinear behaviour and seismic vulnerability assessment of corroded structures subject to MS-AS ground motion sequences.

Appendix A: Summary of the constructed real MS-AS ground motion sequences

Details of the MS-AS ground motion database used in the nonlinear dynamic analyses of the current study are provided in Table A1.

Table A1. Details of the selected real MS-AS ground motion sequences

No	NGA Event name/Event ID	Station ID	Magnitude	Distance (km)	V_{S30} (m/s)	PGA† (g)
1	Managua-01 & 02	199	6.24, 5.2	4.06, 7.57	288.77	0.394, 0.287
2	Imperial Valley-06 & 07	118	6.53, 5.01	3.95, 13.86	205.6	0.442, 0.238
3	Imperial Valley-06 & 07	210	6.53, 5.01	2.68, 15.83	223.0	0.671, 0.084
4	Irpinia, Italy-01 & 02	935	6.9, 6.2	10.84, 20.39	1000.0	0.295, 0.076
5*	Coalinga-02 & 04	175	5.09, 5.18	12.44, 12.62	376.1	0.138, 0.154
6*	Coalinga-02 & 04	412	5.09, 5.18	16.71, 14.92	338.5	0.12, 0.179
7*	Chalfant Valley-01 & 02	430	5.77, 6.19	24.33, 21.92	271.4	0.052, 0.19
8	Northridge-01 & 06	315	6.69, 5.28	8.66, 13.51	297.7	0.321, 0.125
9	Northridge-01 & 06	318	6.69, 5.28	29.88, 29.89	297.1	0.205, 0.056
10	Northridge-01 & 04	325	6.69, 5.93	24.76, 19.92	405.2	0.236, 0.152
11	Northridge-01 & 03,	341	6.69, 5.2	15.6, 22.15	257.2	1.564, 0.056
12*	Kocaeli & Duzce, Turkey	709	7.51, 7.14	15.37, 6.58	276.0	0.323, 0.428
13	Chi-Chi,Taiwan-01 & 02	647	7.62, 5.9	3.14, 46.02	542.6	0.764, 0.044
14	Chi-Chi, Taiwan-01 & 05	749	7.62, 6.2	44.54, 34.87	375.3	0.068, 0.057
15	Chi-Chi, Taiwan-01& 05,	756	7.62, 6.2	53.84, 56.87	272.6	0.098, 0.058
16	Chi-Chi, Taiwan-01 & 05	758	7.62, 6.2	46.95, 35.92	272.6	0.073, 0.05
17	Chi-Chi, Taiwan-01, &05	768	7.62, 6.2	47.76, 57.18	272.6	0.08, 0.064,
18	Chi-Chi, Taiwan-01 & 05	769	7.62, 6.2	58.05, 44.98	272.6	0.071, 0.051
19	Chi-Chi, Taiwan-01, & 02	776	7.62, 5.9,	53.56, 47.41,	272.6	0.155, 0.042,
20	Chi-Chi, Taiwan-01 & 05	1035	7.62, 6.2	16.62, 68.07	272.6	0.118, 0.042
21	Chi-Chi, Taiwan-01, &02,	1064	7.62, 5.9	17.18, 55.69,	473.9	0.122, 0.04
22	K-KiK-NET 3196 & 3210	IWTH26	6.87, 5.50	8.74, 30.17	371.1	0.925, 0.190
23	K-KiK-NET 4093, 4101	CHB007	9.08, 7.89	34.07, 91.66	264.0	0.633, 0.215
24	K-KiK-NET 4093, 4095	IBR003	9.08, 5.80	65.83, 123.26	295.1	1.304, 0.243

†The values of PGA listed in this table are taken from the PEER-NGA and K-NET/KiK-net database flat files.

*Records with $PGA_{AS}/PGA_{MS} > 1$

References

ACI. (2002). Building code requirements for structural concrete. ACI 318-02, American Concrete Institute, Farmington Hills.

Acito, M., Bocciarelli, M., Chesi, C., Milani, G. (2014). Collapse of the clock tower in Finale Emilia after the May 2012 Emilia Romagna earthquake sequence: Numerical insight. Engineering Structures, 72, 70-91. https://doi.org/10.1016/j.engstruct.2014.04.026.

Acito, M., Magrinelli, E., Milani, G., Tiberti, S. (2020). Seismic vulnerability of masonry buildings: Numerical insight on damage causes for residential buildings by the 2016 central Italy seismic sequence and evaluation of strengthening techniques. Journal of Building Engineering, 28, https://doi.org/10.1016/j.jobe.2019.101081.

Afsar Dizaj, E., Kashani, M.M. (2020). Numerical investigation of the influence of cross-sectional shape and corrosion damage on failure mechanisms of RC bridge piers under earthquake loading. Bulletin of Earthquake Engineering, 18, 4939–4961. https://doi.org/10.1007/s10518-020-00883-3

Afsar Dizaj, E., Madandoust, R., Kashani, M.M. (2018a). Exploring the impact of chloride-induced corrosion on seismic damage limit states and residual capacity of reinforced concrete structures. Structure and Infrastructure Engineering, 14(6), 714–729. https://doi.org/10.1080/15732479.2017.1359631.

Afsar Dizaj, E., Madandoust, R., Kashani, M.M. (2018b). Probabilistic seismic vulnerability analysis of corroded reinforced concrete frames including spatial variability of pitting corrosion. Soil Dynamics and Earthquake Engineering, 114, 97–112. https://doi.org/10.1016/j.soildyn.2018.07.013.

Alipour, A., Shafei, B., Shinozuka, M. (2011). Performance evaluation of deteriorating highway bridges located in high seismic areas. Journal of Bridge Engineering, 6, 597-611. https://doi.org/10.1061/(ASCE)BE.1943-5592.0000197.

Apostolopoulos, C.A., Papadakis, V.G. (2008). Consequences of steel corrosion on the ductility properties of reinforcement bar. Construction and Building Materials, 22(12), 2316-2324. https://doi.org/10.1016/j.conbuildmat.2007.10.006.

ASCE-7. (2002). Minimum design loads for buildings and other structures. Structural Engineering Institute.

Baker, J.W., Cornell, C.A. (2008). Vector-valued Intensity Measures Incorporating Spectral Shape For Prediction of Structural Response. Journal of Earthquake Engineering, 12(4), 534–54. https://doi.org/10.1080/13632460701673076.

Baker, J. (2011). Conditional mean spectrum: tool for ground-motion selection. Journal of Structural Engineering, 137 (3), 322-331. https://doi.org/10.1061/(ASCE)ST.1943-541X.0000215.

Banerjee, S., Vishwanath, B.S., Devendiran, D.K. (2019). Multihazard resilience of highway bridges and bridge networks: a review. Structure and Infrastructure Engineering., 15(12), 1694-1714. https://doi.org/10.1080/15732479.2019.1648526.

Capacci, L., Biondini, F. (2020). Probabilistic life-cycle seismic resilience assessment of aging bridge networks considering infrastructure upgrading. Structure and Infrastructure Engineering, 16(4), 659-675. https://doi.org/10.1080/15732479.2020.1716258.

Capacci, L., Biondini, F., Titi, A. (2019). Lifetime seismic resilience of aging bridges and road networks. Structure and Infrastructure Engineering., 16(2), 266-286. https://doi.org/10.1080/15732479.2019.1653937.

Chase, R.E., Liel, A.B., Luco, N., Baird, B.W. (2019). Seismic loss and damage in light-frame wood buildings from sequences of induced earthquakes, Earthquake Engineering and Structural Dynamics, 48(12), 1365-1383. https://doi.org/10.1002/eqe.3189.

Coronelli, D., Gambarova, P. (2004). Structural assessment of corroded reinforced concrete beams: modelling guidelines. Journal of Structural Engineering., 130 (8), 1214-1224. https://doi.org/10.1061/(ASCE)0733-9445(2004)130:8(1214).

Cui, Z., Alipour, A., Shafei, B. (2019). Structural performance of deteriorating reinforced concrete columns under multiple earthquake events. Engineering Structures, 191, 460–468. https://doi.org/10.1016/j.engstruct.2019.04.073.

Cui, F., Zhang, H., Ghosn, M., Xu, Y. (2018). Seismic fragility analysis of deteriorating RC bridge substructures subject to marine chloride-induced corrosion. Soil Dynamics and Earthquake Engineering, 155, 61-72. https://doi.org/10.1016/j.engstruct.2017.10.067.

Du, Y.G., Clark, L.A., Chan, A.H.C. (2005a). Residual capacity of corroded reinforcing bars. Magazine of Concrete Research, 57(3), 135–147. https://doi.org/10.1680/macr.2005.57.3.135.

Du, Y.G., Clark, L.A., Chan, A.H.C. (2005b). Effect of corrosion on ductility of reinforcing bars. Magazine of Concrete Research, 57(7), 407–419. https://doi.org/10.1680/macr.2005.57.7.407.

Ebrahimian, H., Jalayer, F., Asprone, D., Lombardi, AM., Marzocchi, W., Prota, A., Manfredi, G. (2014). A performance-based framework for adaptive seismic aftershock risk assessment. Earthquake Engineering and Structural Dynamics, 43(14), 2179-2197. https://doi.org/10.1002/eqe.2444.

FHWA. (2015). NBI ASCII Files - NBI - Programs - Integrated - Bridge - FHWA. https://www.fhwa.dot.gov/bridge/nbi/ascii.cfm.

Ge, X., Dietz, M.S., Alexander, N.A. *et al.* (2020). Nonlinear dynamic behaviour of severely corroded reinforced concrete columns: shaking table study. Bulletin of Earthquake Engineering, 18, 1417–1443. https://doi.org/10.1007/s10518-019-00749-3.

Goda, K. (2012). Nonlinear response potential of mainshock–aftershock sequences from Japanese earthquakes. Bulletin of the Seismological Society of America, 102(5), 2139–2156. https://doi.org/10.1785/0120110329.

Goda, K. (2015). Record selection for aftershock incremental dynamic analysis, Earthquake Engineering and Structural Dynamic., 44(7), 1157–1162. https://doi.org/10.1002/eqe.2513.

Goda, K., Salami, R. (2014). Inelastic seismic demand estimation of wood-frame houses subjected to mainshock-aftershock sequences. Bulletin of Earthquake Engineering, 12(2), 855–874. https://doi.org/10.1007/s10518-013-9534-4.

Goda, K., Taylor, C.A. (2012). Effects of aftershocks on peak ductility demand due to strong ground motion records from shallow crustal earthquakes. Earthquake Engineering and Structural Dynamics, 41(15), 2311–30. https://doi.org/10.1002/eqe.2188.

Guo, A., Yuan, W., Lan, C.h., Guan, X., Li, H. (2015). Time-dependent seismic demand and fragility of deteriorating bridges for their residual service life. Bulletin of Earthquake Engineering, 13(8), 2389-2409. https://doi.org/10.1007/s10518-014-9722-x.

Hatzigeorgiou, G. D., Liolios, A. A. (2010). Nonlinear behaviour of RC frames under repeated strong ground motions. Soil dynamics and earthquake engineering, 30(10), 1010-1025. https://doi.org/10.1016/j.soildyn.2010.04.013.

Hatzivassiliou, M., & Hatzigeorgiou, G. D. (2015). Seismic sequence effects on three-dimensional reinforced concrete buildings. Soil Dynamics and Earthquake Engineering, 72, 77-88. https://doi.org/10.1016/j.soildyn.2015.02.005.

HAZUS-MH MR5. (2010). Earthquake loss estimation methodology. Technical and User's Manual. Department of Homeland Security, Federal Emergency Management Agency, Mitigation Division. Washington D.C.

Hosseinpour, F., Abdelnaby, A. E. (2017). Effect of different aspects of multiple earthquakes on the nonlinear behavior of RC structures. Soil Dynamics and Earthquake Engineering, 92, 706-725. https://doi.org/10.1016/j.soildyn.2016.11.006.

Iervolino, I., Chioccarelli, E., Suzuki, A. (2020). Seismic damage accumulation in multiple mainshock–aftershock sequences. Earthquake Engineering and Structural Dynamics, 49(10), 1007-1027. https://doi.org/10.1002/eqe.3275.

Jalayer, F., Asprone, D., Prota, A., Manfredi, G. (2011). A decision support system for post-earthquake reliability assessment of structures subjected to aftershocks: an application to L'Aquila earthquake, 2009. Bulletin of Earthquake Engineering, 9, 997–1014. https://doi.org/10.1007/s10518-010-9230-6.

Jeon, J.S., DesRoches, R., Lowes, L.N., Brilakis, I. (2015). Framework of aftershock fragility assessment-case studies: older California reinforced concrete building frames. Earthquake Engineering and Structural Dynamics, 44(15), 2617–36. https://doi.org/10.1002/eqe.2599.

Kashani., M. M., Ge, X., Dietz, M. S., Crewe, A. J., Alexander, N. A. (2019). Significance of non-stationary characteristics of ground-motion on structural damage: shaking table study. Bulletin of Earthquake Engineering, 17(9), 4885-4907. https://doi.org/10.1007/s10518-019-00668-3.

Kashani, M. M., Málaga-Chuquitaype, C., Yang, S., & Alexander, N. A. (2017). Influence of non-stationary content of ground-motions on nonlinear dynamic response of RC bridge piers. Bulletin of Earthquake Engineering, 15(9), 3897-3918. https://doi.org/10.1007/s10518-017-0116-8.

Kashani, M.M., Barmi, A.K., Malinova, S. (2015b). Influence of inelastic buckling on low-cycle fatigue degradation of reinforcing bars. Construction and Building Materials, 94, 644–655. https://doi.org/10.1016/j.conbuildmat.2015.07.102.

Kashani, M.M., Lowes, L.N., Crewe, A.J., Alexander, N.A. (2015a). Phenomenological hysteretic model for corroded reinforcing bars including inelastic buckling and low-cycle fatigue degradation. Computer and Structures, 156, 58-71. https://doi.org/10.1016/j.compstruc.2015.04.005.

Kashani, M.M., Lowes, L.N., Crewe, A.J., Alexander, N.A. (2016). Nonlinear fibre element modelling of RC bridge piers considering inelastic buckling of reinforcement. Engineering Structures., 116, 163-177. https://doi.org/10.1016/j.engstruct.2016.02.051.

Lee, G.C., Mohan, S.B., Huang, C., Fard, B.N. (2013). A study of U.S. Bridge failures. MCEER Earthquake Engineering to Extreme Events.

Li, Q., Ellingwood, B.R. (2007). Performance evaluation and damage assessment of steel frame buildings under mainshock–aftershock earthquake sequence. Earthquake Engineering and Structural Dynamics ,36(3), 405–427. DOI: 10.1002/eqe.667.

Manafpour, A.R., and Moghaddam, P.K. (2019). Performance capacity of damaged RC SDOF systems under multiple far- and near-field earthquakes. Soil Dynamics and Earthquake Engineering, 116, 164-173. https://doi.org/10.1016/j.soildyn.2018.09.045.

Manson, S.S. (1965). Fatigue: a complex subject – some simple approximations. Experimental Mechanics, 5(7), 193–226. https://doi.org/10.1007/BF02321056.

McKenna, F. (2011). OpenSees: a framework for earthquake engineering simulation. Computing in Science & Engineering, 13(4), 58-66. DOI: 10.1109/MCSE.2011.66.

Miner, M.A. (1945). Cumulative damage in fatigue. Transactions of the ASME, Series E. Journal of Applied Mechanics, 12, 159–164.

Naderpour, H., Vakili, K. (2019). Safety assessment of dual shear wall-frame structures subject to Mainshock-Aftershock sequence in terms of fragility and vulnerability curves. Earthquakes and Structures, 16(4), 425-436. http://dx.doi.org/10.12989/eas.2019.16.4.425.

Otieno, M., Beushausen, H., Alexander, M. (2016a). Chloride-induced corrosion of steel in cracked concrete – Part I: Experimental studies under accelerated and natural marine environments. Journal of Cement and Concrete Research, 79, 373–85. https://doi.org/10.1016/j.cemconres.2015.08.009.

Otieno, M., Beushausen, H., Alexander, M. (2016b). Chloride-induced corrosion of steel in cracked concrete—Part II: Corrosion rate prediction models. Journal of Cement and Concrete Research, 79, 386–94. https://doi.org/10.1016/j.cemconres.2015.08.008.

Panchireddi, B., Ghosh, J. (2019). Cumulative vulnerability assessment of highway bridges considering corrosion deterioration and repeated earthquake events. Bulletin of Earthquake Engineering, 17, 1603–1638. https://doi.org/10.1007/s10518-018-0509-3.

Priestley, M., Paulay, T. (1992). Seismic design of reinforced concrete and masonry buildings. New York: John Wiley & Sons, Inc.

Raghunandan, M., Liel, A.B., Luco, N. (2015). Aftershock collapse vulnerability assessment of reinforced concrete frame structures. Earthquake Engineering and Structural Dynamics, 44, 419–439. https://doi.org/10.1002/eqe.2478.

Reggia, A., Morbi, A., Plizzari, G.A. (2020). Experimental study of a reinforced concrete bridge pier strengthened with HPFRC jacketing. Engineering Structures, 210, https://doi.org/10.1016/j.engstruct.2020.110355.

Ryu, H., Luco, N., Uma, S.R., Liel, A.B. (2011). Developing fragilities for mainshock-damaged structures through incremental dynamic analysis. 9th Pacific Conference on Earthquake Engineering, Auckland, New Zealand.

Salami, M.R., Kashani, M.M., Goda, K. (2019). Influence of advanced structural modeling technique, mainshock-aftershock sequences, and ground-motion types on seismic fragility of low-rise RC structures. Soil Dynamics and Earthquake Engineering, 11, 263-279 https://doi.org/10.1016/j.soildyn.2018.10.036.

Scott, B.D., Park, R., Priestley, M.J.N. (1982). Stress–strain behavior of concrete confined by overlapping hoops at low and high strain rates. ACI Structural Journal, 99(2), 13–27.

Shcherbakov, R., Turcotte, D.L., Rundle, J.B. (2005). Aftershock statistics. Pure and Applied Geophysics, 162(6–7), 1051–1076. https://doi.org/10.1007/s00024-004-2661-8.

Stewart, M.G., Suo, Q. (2009). Extent of spatially variable corrosion damage as an indicator of strength and time-dependent reliability of RC beams. Engineering Structures, 31, 198-207. https://doi.org/10.1016/j.engstruct.2008.08.011.

Titi, A., Bianchi, S., Biondini, F., Frangopol, D.M. (2018). Influence of the exposure scenario and spatial correlation on the probabilistic life-cycle seismic performance of deteriorating RC frames. Structure and Infrastructure Engineering, 14(7), 986-996. https://doi.org/10.1080/15732479.2018.1438481.

Uriz, P. (2005). Towards Earthquake Resistant Design of Concentrically Braced Steel Structures. PhD thesis, University of California, Berkeley, CA, USA.

Val, D. V. (2007). Factors affecting life-cycle cost analysis of RC structures in chloride contaminated environments. Journal of Infrastructure Systems, 13, 135–143. https://doi.org/10.1061/(ASCE)1076-0342(2007)13:2(135).

Vamvatsikos, D., Cornell, C.A. (2002). Incremental dynamic analysis. Earthquake Engineering and Structural Dynamics, 31(3), 491–514. DOI: 10.1002/eqe.141.

Vamvatsikos, D., Cornell, C.A. (2005). Developing efficient scalar and vector intensity measures for IDA capacity estimation by incorporating elastic spectral shape information. Earthquake Engineering and Structural Dynamics, 34(13), 1573–600. https://doi.org/10.1002/eqe.496.

Virmani, Y.P. (2002). Corrosion costs and preventive strategies in the United States. NACE Org. Available online at: https://www.nace.org/uploadedfiles/publications/ccsupp.pdf.

Vu, K. A. T., Stewart, M. G. (2000). Structural reliability of concrete bridges including improved chloride-induced corrosion models. Structural Safety, 22, 313–333. https://doi.org/10.1016/S0167-4730(00)00018-7.

Wallbank, E.J. (1989). The performance of concrete bridges: a survey of 200 highway bridges. London: HMSO Publication.

Xu, J., Wu, G., Feng, D., Cotsovos, D.M., Lu, Y. (2020). Seismic fragility analysis of shear-critical concrete columns considering corrosion induced deterioration effects. Soil Dynamics and Earthquake Engineering, 134: https://doi.org/10.1016/j.soildyn.2020.106165.

Zhao, J., Sritharan, S. (2007). Modeling of strain penetration effects in fiber-based analysis of reinforced concrete structures. ACI Structural Journal, 104(2), 133–41.